RSC Advances

PAPER

View Article Online
View Journal | View Issue

Cite this: *RSC Adv.*, 2026, **16**, 6078

Impact of functionalization linker chemistry on cellulase immobilization: a comparative study of TEOS, APTS, and MPTS functionalized magnetic nanoparticles

Larissa Lamburghini Brandão,[ab] Thais de Andrade Silva,[ab] Ana Carolina de Lima Barizão,[a] Larissa Bernardino Moro,[a] Julyana Noval de Souza Ferreira,[c] Chadia Chahud Maestrello,[d] André Romero da Silva,[c] Laura Marina Pinotti,[b] Ruchi Gupta,[e] Sérvio Tulio Alves Cassini[a] and Jairo Pinto de Oliveira *[ab]

Magnetic nanobiocatalysts based on Fe_3O_4 nanoparticles coated with tetraethyl orthosilicate (TEOS) and functionalised with (3-aminopropyl)triethoxysilane (APTS) or (3-mercaptopropyl)trimethoxysilane (MPTS) were developed for cellulase immobilisation and systematically evaluated. Physicochemical characterisation confirmed successful surface modification, while adsorption studies showed that MNPs@TEOS-MPTS achieved the highest immobilisation capacity (q_e = 1.06 mg mg^{-1}) with fast kinetics following a pseudo-second-order model, whereas MNPs@TEOS-APTS displayed lower loading (q_e = 0.94 mg mg^{-1}) and diffusion-limited behaviour. Enzymatic assays revealed that MNPs@TEOS-APTS exhibited the highest catalytic activity (1.92 U g^{-1}) under optimal conditions (pH 5, 50 °C), but with reduced tolerance to alkaline pH, while MNPs@TEOS-MPTS showed slightly lower initial activity (1.61 U g^{-1}) combined with enhanced thermal resistance and operational stability. Reusability tests highlighted MNPs@TEOS–MPTS as the most robust system, retaining 62% of its initial activity after six cycles, compared to 33% for MNPs@TEOS–APTS and 52% for MNPs@TEOS. Molecular docking analysis supported these findings, indicating higher binding affinity for APTS associated with favourable catalytic orientation, whereas MPTS promoted multiple stabilising interactions that increased conformational rigidity. Overall, the results demonstrate that ligand chemistry critically governs the balance between catalytic efficiency and long-term stability, providing rational guidelines for the design of magnetic nanobiocatalysts tailored to industrial applications.

Received 30th September 2025
Accepted 4th January 2026

DOI: 10.1039/d5ra07440a

rsc.li/rsc-advances

Introduction

The enzymatic degradation of plant biomass plays a pivotal role in the sustainable transition toward bio-based economies. Cellulases, classified as hydrolases targeting glycosidic bonds, are the cornerstone of this process.[1] These enzymes are essential across various industrial sectors, ranging from second-generation biofuel production to textile biopolishing and paper manufacturing, owing to their ability to hydrolyze cellulose into fermentable sugars like glucose and cellobiose.[2,3] However, their large-scale implementation faces significant technoeconomic bottlenecks, primarily due to the intrinsic instability of free enzymes under fluctuating pH and temperature conditions, as well as the difficulty of recovery for repeated use.[4,5]

To address these limitations, enzyme immobilization on solid supports has emerged as a robust strategy to enhance catalytic stability and facilitate biocatalyst recycling.[6,7] The selection of both the support material and the immobilization protocol is critical, as these factors directly govern protein loading, activity retention, and resistance to operational stress.[8,9] In this context, magnetic iron oxide nanoparticles (FeMNPs) have garnered significant attention. Their high surface-to-volume ratio, biocompatibility, and susceptibility to external magnetic fields allow for rapid and energy-efficient separation, overcoming the mass transfer limitations of traditional supports.[10,11]

Beyond their potential in biocatalysis, FeMNPs have been extensively explored in diverse fields, ranging from environmental remediation to advanced sensing platforms.[12–14] Recent studies have highlighted the versatility of Fe_3O, based composites in selective adsorption and catalytic applications, demonstrating their robustness as functional materials.[12–14]

[a]*Center for Research, Innovation and Development of Espírito Santo - CPID, Espírito Santo, Brazil. E-mail: jairo.oliveira@ufes.br*
[b]*Federal University of Espírito Santo - UFES, Espírito Santo, Brazil*
[c]*Federal Institute of Espírito Santo - IFES, Espírito Santo, Brazil*
[d]*University of São Paulo - USP, São Paulo, Brazil*
[e]*School of Chemistry, University of Birmingham, Birmingham, UK*

Crucially, the surface modulation of these magnetic cores, particularly *via* aminosilanization strategies, has proven effective in enhancing chemical stability and optimizing interfacial interactions in non-enzymatic systems as well.[12–14] These successful applications in broader chemical contexts reinforce the rationale for employing silane-based surface engineering to develop high-performance nanobiocatalysts.

However, to utilize FeMNPs effectively for hydrolases like cellulase, specific control over the surface chemistry is required to prevent denaturation and ensure proper orientation. In this work, we draw upon these surface functionalization principles to investigate cellulase immobilization using three distinct silane agents: tetraethyl orthosilicate (TEOS), (3-aminopropyl) triethoxysilane (APTS), and (3-mercaptopropyl)triethoxysilane (MPTS). While aminosilanization (APTS) and other functionalization methods have shown promise in stabilizing diverse systems, their specific impact on the structural conformation of immobilized cellulases remains under-explored.

Therefore, we present a systematic investigation characterizing the immobilized enzymes under different pH and temperature conditions. Furthermore, we integrated molecular docking simulations to elucidate the atomistic interactions between cellulases and the functionalization linkers. This combined experimental and computational approach aims to identify the strategy that maximizes both catalytic efficiency and biocatalyst lifespan, providing fundamental insights for the rational design of robust industrial biocatalysts.

Experimental

Materials

Ferrous chloride tetrahydrate ($FeCl_2 \cdot 4H_2O$, Sigma-Aldrich 44939), ferric chloride hexahydrate ($FeCl_3 \cdot 6H_2O$, Sigma-Aldrich F2877), ammonium hydroxide (NH_4OH, Prochemios), sodium citrate ($Na_3C_6H_5O_7$, Dynamica – 1146), tetraethyl orthosilicate (TEOS, Sigma-Aldrich – 86578), (3-aminopropyl) triethoxysilane (APTS, Sigma-Aldrich – 440140), (3-mercaptopropyl)trimethoxysilane (MPTS, Sigma-Aldrich – 175617), ethanol (Exodus, Brazil), argon gas (Oxivit, 99.999%), ultrapure water (Millipore Synergy Merck), neodymium magnet 50 × 50 × 12 mm (Supermagnet, Brazil), cellulase from *Aspergillus* sp., aqueous solution (Sigma-Aldrich – C2605), sodium phosphate monobasic (NaH_2PO_4, Synth – 01F2002.01.AF), sodium phosphate dibasic dihydrate ($Na_2HPO_4 \cdot 2H_2O$, Synth – 01F1032.01.AG), sodium chloride (NaCl, Synth – 01C1060.01.AG), Coomassie Brilliant Blue BG-250 (Merck – C.I. 42655), orthophosphoric acid 85% (Neon – 00232-DSYS), glutaraldehyde (Electron Microscopy Sciences – 16200), sodium acetate trihydrate P.A. ($C_2H_3NaO_2 \cdot 3H_2O$, Neon – 00083), glacial acetic acid P.A. ACS (CH_3COOH, Vetec – 2789), sodium carbonate (Na_2CO_3, Fluka – 71347-25G), sodium bicarbonate ($NaHCO_3$, Sigma-Aldrich – 56014-25G), 3,5-dinitrosalicylic acid P.A. (DNS, Neon – 02938), sodium potassium tartrate tetrahydrate P.A. ($C_4H_4KNaO_6 \cdot 4H_2O$, Neon – 02368), sodium carboxymethylcellulose (CMC, Neon – 00803). In addition, all glassware was cleaned with aqua regia (3 HCl : 1 HNO_3) and rinsed ten times with ultrapure water prior to the experiments.

Synthesis and functionalization of magnetic nanoparticles

The MNPs synthesis and functionalization followed the methodology adapted from Andrade Silva *et al.* [15] and Thangaraj *et al.*[16] Briefly, the nanomaterials were synthesized through coprecipitation of iron salts ($FeCl_2 \cdot 4H_2O$ 0.09 M and $FeCl_3 \cdot 6H_2O$ 0.18 M) in a basic medium (12 mL of NH_4OH, at a flow rate of 5 mL min^{-1}) at 65 °C under an argon atmosphere. The nanoparticles were subsequently stabilized with 2.75 g of sodium citrate at 90 °C for 30 minutes. After this period, the reaction was stopped with an ice bath, and the MNPs were washed three times with 10 mL of ethanol and stored in Falcon tubes (4 °C) until characterization.

For the stabilization of nanoparticles with TEOS, an external magnetic field was applied to 10 mL of the MNPs suspension, aiming to precipitate the MNPs, and the supernatant was removed. Subsequently, a solution of 13.34 mL of ultrapure water and 53.51 mL of ethanol was added to the pellet, which was then sonicated for 30 minutes. Afterwards, 2.7 mL of TEOS and 13.34 mL of NH_4OH (28% v/v) were added, and the solution was kept under agitation (180 rpm) for 18 hours at 28 °C. After this period, the stabilized MNPs (MNPs@TEOS) were washed ten times to remove all excess TEOS, and the functionalization process was then carried out.

For functionalization with APTS and MPTS, 15 mL of MNPs@TEOS were left under the influence of an external magnetic field until the nanoparticles completely precipitated, and the supernatant was then removed. The MNPs@TEOS were then resuspended in 15 mL of an ethanolic solution containing the desired functionalizing agent (80 mg mL^{-1}) and sonicated for 30 minutes. Subsequently, the solution was kept under agitation (180 rpm) for 2 hours at 28 °C to complete the functionalization process. The nanoparticles functionalized with MPTS (MNPs@TEOS–MPTS) were then washed until the excess functionalizing agent was removed entirely. In the specific case of APTS (MNPs@TEOS–APTS), an additional crosslinking step was performed using 2.5% glutaraldehyde in phosphate buffer (pH 7.2) for 2 hours. All functionalized materials were subjected to successive washings to remove residual reagents and subsequently stored at 4 °C.

Characterization of magnetic nanoparticles

The MNPs (both bare and functionalized) were characterized to determine their morphology and assess the efficiency of the functionalization process. For this purpose, UV-visible absorption spectroscopy, X-ray diffraction (XRD), Transmission Electron Microscopy (TEM), Raman spectroscopy, Fourier-Transform Infrared spectroscopy (FTIR), zeta potential and energy-dispersive X-ray spectroscopy (EDS) were used. The obtained data was processed using OriginPro 8.5 SR1 and GraphPad Prims 6 software.

Enzyme activity and characterization

Enzymatic activity was determined using the Miller (1959) method for quantifying reducing sugars. Cellulase enzymes break cellulose into reducing sugars. This implies that the

concentration of reducing sugars is indicative of cellulase enzyme activity. In the Miller method, the concentration of reducing sugars is determined by a condensation reaction between the reducing groups of sugars and the nitro groups present in the 3,5-dinitrosalicylic acid (DNS) reagent, resulting in intensely brown-coloured products that can be quantified using spectrophotometry at 540 nm. The calculation of enzymatic activity was estimated in units (U mg^{-1}) using the concept of activity (μmol min^{-1}) along with the standard curve,[18] thus obtaining eqn (1) below.

$$\text{U g}^{-1} = \frac{(ABS_{540\ \text{nm}} - b)\ V_{\text{DNS}} \left(\frac{V_{\text{rea}}}{V_{\text{ali}}}\right)}{a\ t\ m_{\text{sup}}} \quad (1)$$

where: ABS_{540nm} – corrected absorbance of the sample at 540 nm. b – intercept of the standard curve. V_{DNS} – final volume in the DNS analyse (mL). V_{rea} – total volume of enzymatic assay (mL). V_{ali} – sample volume taken from the reaction (mL). a – slope of the standard curve (Abs mL μmol^{-1}). t – reaction time (min). m_{sup} – mass of support with immobilized enzyme (g); for free enzyme, use enzyme mass (g).

Free enzymes

The assays with free cellulases (not conjugated to nanoparticles) were performed by adding 100 μL of a cellulase solution (100 mg mL^{-1}) to 900 μL of 1% carboxymethylcellulose (CMC) and under varying of incubating (0, 1, 2, 3, 4, 5, 10, 15, 20 e 30 min), temperature (30, 40, 50, 60 e 70 °C) and pH (4, 5, 6, 7, 8 e 9). After incubation, 100 μL of each sample was mixed with 100 μL of DNS (44 mM) and heated at 100 °C for 5 min. The samples were then diluted to a final volume of 2 mL, and absorbance was measured at 540 nm using a spectrophotometer. For the temperature assays, the pH of the free enzyme was maintained at its optimal value (pH 5), while for the pH variation assays, the temperature was maintained at the optimal value (50 °C), as reported in the literature.[4,5,22]

Bioconjugated nanoparticles

To determine the enzymatic activity of bioconjugated nanoparticles (MNPs@TEOS, MNPs@TEOS–APTS and MNPs@TEOS–MPTS), 20 mg of each nanoconjugate was separately resuspended in 100 μL of ultrapure water. Subsequently, 500 μL of CMC (0.1%) was added to each vial and the mixture was kept under agitation for 10 minutes. Subsequently, each sample (100 μL), collected with the aid of a neodymium magnet, was mixed with 100 μL of DNS (44 mM) and heated at 100 °C for 5 minutes. The samples were then diluted to reach a final volume of 2 mL, and absorbance was measured using a spectrophotometer (540 nm). We varied the temperature in 30, 40 and 50 °C, and pH in 5, 7 and 9. As with the free enzymes, for temperature variation assays, the optimal pH of the free enzyme (pH 5) was fixed, while for pH variation assays, the optimal temperature of the free enzyme (50 °C) was maintained.

Recyclability (residual activity)

The enzymatic activity of the conjugates was evaluated over six reuse cycles, in which the materials were separated with an external magnetic field for 5 min after each reaction. Between cycles, the bioconjugates were washed with acetate buffer (100 mM, pH 5) to remove the remaining reaction medium.

Molecular docking

The three-dimensional structures of the enzyme were obtained from the Protein Data Bank server (https://www.rcsb.org, code 1ks5) (Berman, 2000), rendered and visualized using PyMol Molecular Graphics System (Version 2.4.1, Schrödinger, LLC Pymol). For the TEOS, APTS, and MPTS functionalization linkers, three-dimensional structures were prepared and geometrically optimized using Avogadro 1.2.0 software with the UFF force field. Subsequently, the protonation state of each ligand was verified in MarvinSketch 20.20, and the structures underwent semi-empirical optimizations in MOPAC 2016 using the PM7 method. Following optimization, electrostatic charges were added to the molecules using Chimera 1.14.

For the molecular docking step, the enzyme was prepared as a receptor in AutoDockTools v.1.5.6, where polar hydrogens and Kollman charges were added. The functionalization linkers, in turn, were assigned Gasteiger charges, and their bonds were defined as non-rotatable. The docking simulation was configured with a cubic grid box centred on the enzyme, measuring 122 × 122 × 122 points with a spacing of 0.375 Å. Calculations were performed using AutoDock4 with the Lamarckian genetic algorithm, involving 10 independent simulations for each ligand, resulting in a total of 100 conformations. The conformation with the lowest binding energy (ΔG binding) was selected for each complex, as more negative values indicate higher molecular affinity. Finally, molecular interactions between the enzyme and functionalization linkers were analysed and visualized in Discovery Studio Visualizer 2021, enabling identification of binding sites, interaction types (such as hydrogen bonds, hydrophobic interactions, and electrostatic interactions), and evaluation of the stability of the formed complexes. This computational approach enabled the prediction of binding affinity and interaction modes between the enzyme and the studied compounds, providing insights into their potential applications.

Adsorption kinetics

The kinetic assays for cellulase immobilization on MNPs were performed following protocols adapted from the studies of [NO_PRINTED_FORM][19] and [NO_PRINTED_FORM].[20] For this purpose, 10 mg of nanoparticles resuspended in 1 mL of PBS buffer (pH 7.2) were mixed with 1 mL of cellulase (50 mg mL^{-1}). The solution was kept under agitation (150 rpm) for different reaction times (1, 2, 3, 6, 12, and 24 h) at a temperature of 28 °C. At the end of each reaction, the MNPs were magnetically separated, and the enzymes in the supernatant were quantified using the Bradford method (595 nm). The mass of enzyme

immobilized per unit mass of MNPs (q_{exp}) was calculated based on eqn (2).

$$q_{exp} = \frac{C_0 - C_e}{m} V \quad (2)$$

where C_0 and C_e are the initial and final enzyme concentrations in the supernatant (mg L^{-1}), respectively, V is the total solution volume (L), and m is the mass of nanoparticles used (mg). The pseudo-first-order and pseudo-second-order kinetic models (eqn (3) and (4), respectively) were applied to obtain insights into the adsorption process (eqn (3) and (4)).

$$q_t = q_e(1 - \exp - K_1 t) \quad (3)$$

$$q_t = \frac{K_2 q_e^2 t}{1 + K_2 q_e t} \quad (4)$$

Results and discussion

Characterization of magnetic nanoparticles (MNPs)

The precipitate obtained from the reduction of iron salts was responsive to an external magnetic field, indicating the formation of MNPs. This was further confirmed by UV-vis spectroscopy through broad-spectrum light absorption and characteristic iron oxide absorption in the ultraviolet region, as shown in Fig. 1A.[21,22] XRD analysis (Fig. 1B) confirmed the formation of magnetite (Fe_3O_4) MNPs, with crystal planes preserved throughout stabilization and functionalization steps.[8,23]

Diameter measurements of 1000 MNPs yielded an average size of 9.47 ± 2.15 nm with uniform size distribution, as shown in the histogram in Fig. 1C. TEM imaging (Fig. 1D) revealed relatively spherical MNPs morphology, consistent with XRD results (Fig. 1B). The small dimensions of the support material enhance enzyme immobilization efficiency due to the increased specific surface area.[5] When combined with monodispersing, these properties enable more realistic models for optimizing nanoscale properties.[24]

Notably, MNPs agglomeration was observed, resulting from inherent magnetic properties through dipole–dipole interactions and van der Waals forces that reduce MNPs stability and promote cluster formation.[8,21–23,25]

Functionalization of magnetic nanoparticles

The functionalization of magnetic nanoparticles (MNPs) plays a crucial role in enzyme immobilization, providing colloidal stability, preventing oxidation of MNPs, and preserving their superparamagnetic characteristics.[8,21,23] Furthermore, functionalization can enable covalent conjugation of cellulases onto MNPs.[22] In this study, MNPs were coated with TEOS, aiming to reduce dipole–dipole interactions and van der Waals forces that lead to particle agglomeration, crystallographic reorientation and oxidation of iron oxide.[8,23] The silica surface stands out as a stabilizer due to its ease of modification for additional functionalization and its stability against temperature and pH variations.[4] The surface modification of MNPs@TEOS with APTS and MPTS functionalization linkers, which contain primary amino (–NH_2) and free thiol (–SH) functional groups, respectively, may contribute to cellulase immobilization (de Andrade Silva *et al.*, 2022).

These functional groups interact with these enzymes due to specific chemic al properties, mediated by forces such as hydrogen bonds, ionic interactions, and covalent bonds.[26]

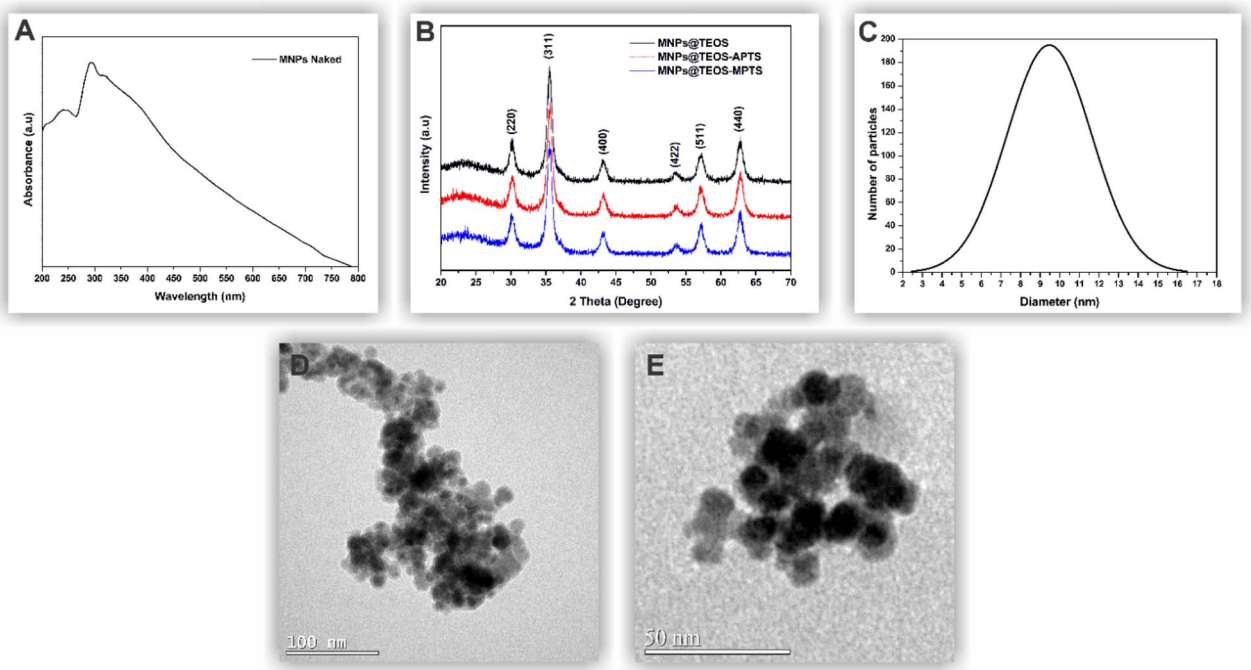

Fig. 1 Characterization of magnetic nanoparticles (MNPs): (A) UV-vis spectrum of bare MNPs; (B) XRD pattern of functionalized MNPs; (C) particle size distribution histogram; (D) and (E) TEM micrographs of MNPs@TEOS.

These interactions facilitate a precise fit between the functional groups of the substrates and the various interaction sites/regions in the enzymes.[26] Common groups in enzyme substrates, such as amino, hydroxyl, carboxyl, and sulphate, establish specific interactions that facilitate biochemical reactions. This complementarity, fundamental for catalytic efficiency and enzyme reaction selectivity, highlights the importance of the multiple interaction regions present in the enzyme structure.[26]

Thus, the functionalization of MNPs performed in this study likely expanded the scope of interaction sites, increasing the chances of interaction between the enzyme's organic groups and the functionalized surface of the MNPs.[22] Raman spectroscopy (Fig. 2A) indicated the success of MNPs functionalization, observed by the peak at 660 cm^{-1}, which is associated with disorder in the iron oxide crystal structure, generally linked to silicon incorporation in its lattice, and the peaks at 1350 cm^{-1} and 1585 cm^{-1}, which are attributed to C–C stretching vibrations present in MNPs with APTS and MPTS.[22,23,27–29]

In Fig. 2B, the presence of the iron oxide core was corroborated by the intense absorption band observed below 700 cm^{-1}, characteristic of the stretching vibrations of the Fe–O bond in the spinel structure. The presence of functional groups from citrate stabilizers, represented by a shift peak from 1540 cm^{-1} up to 1370 cm^{-1} (C–O stretching), and TEOS and functionalizion linkers APTS and MPTS, which are represented by vibrations at 800 cm^{-1}, 860 cm^{-1}, and 1080 cm^{-1} characteristic of silicates and silanes.[22,29–31]

The zeta potential (ZP) values presented in Fig. 2C, provide essential insight into the electrostatic properties of the nanoconjugate surfaces and their colloidal stability in liquid media.[32] Overall, accurate measurement and interpretation of zeta potential provide a robust framework for correlating nanocarrier surface chemistry with catalytic performance and operational stability of immobilised biocatalysts.[8,33]

The MNPs@TEOS, exhibited a strongly negative zeta potential of −39.39 mV. This value is characteristic of silica-based surfaces in aqueous media, where deprotonation of silanol (Si–OH) groups generates a pronounced anionic surface charge.[8,25] Zeta potential magnitudes below −25 mV are widely associated with functionalisation with the aminosilane APTS resulted in a significant neutralisation of surface charge, increasing the zeta potential to −11.46 mV. This reduction in

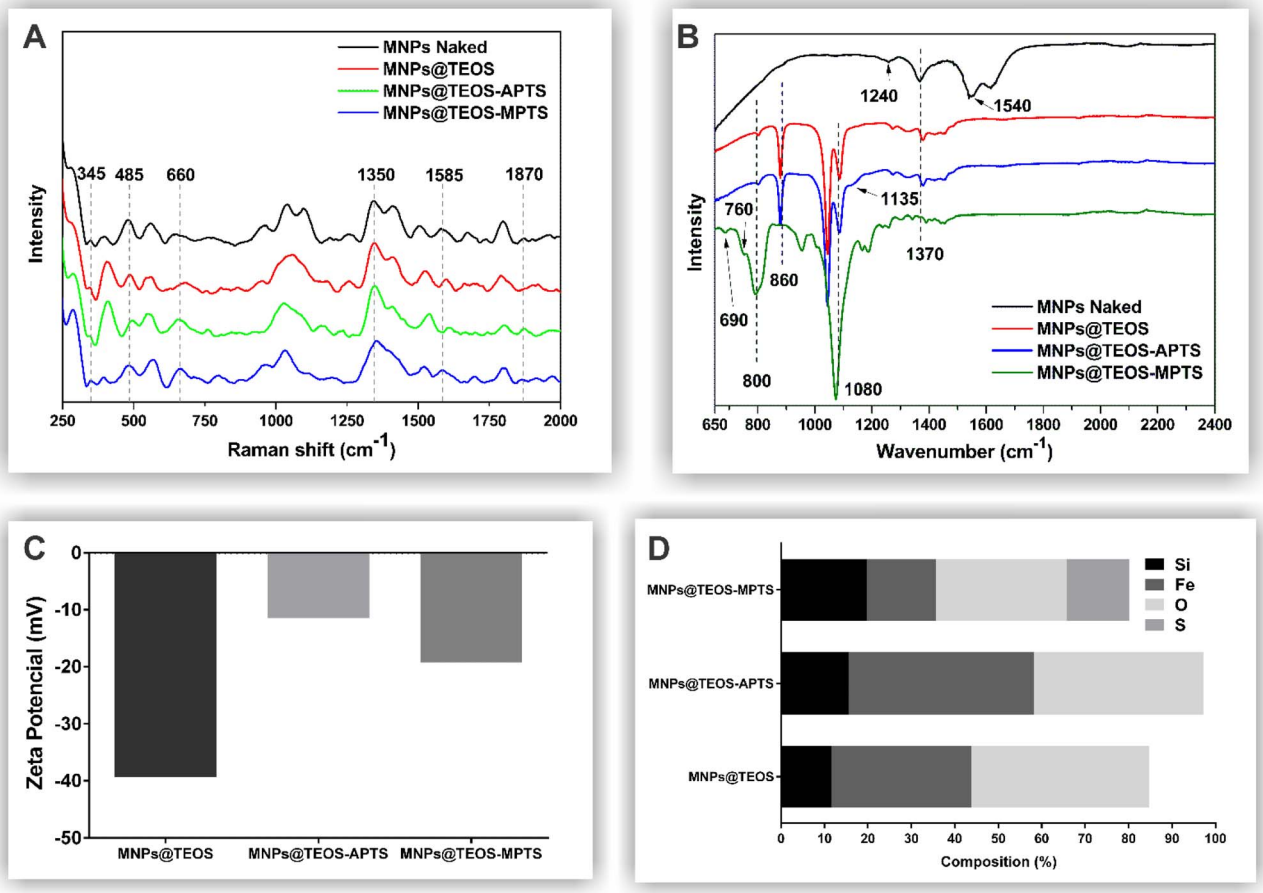

Fig. 2 (A) Raman and (B) infrared spectra of bare magnetic nanoparticles and after each functionalization step for each functionalizer links. (C) Zeta potential measurements of the functionalized MNPs, indicating changes in surface charge density upon modification. (D) Elemental composition analysis (stacked bars) revealing the relative percentages (At.%) of silicon (Si), iron (Fe), oxygen (O), and sulfur (S) for each system, corroborating the successful incorporation of the respective organosilane linkers (TEOS, APTS, and MPTS) onto the magnetic core.

negative ZP magnitude provides clear evidence of successful surface modification.[8] The observed charge neutralisation arises from protonated amino groups ($-NH_3^+$), which counterbalance the anionic charges of the silica shell.[8] Protein immobilisation on amine-functionalised surfaces is frequently favoured near the enzyme isoelectric point, where the net surface charge is minimised.[25]

In contrast, MNPs@TEOS–MPTS displayed an intermediate zeta potential of −19.24 mV, confirming incorporation of the thiol-containing ligand.[15] The less pronounced neutralisation compared to APTS-functionalised samples reflects the distinct electrostatic contribution of thiol terminal groups.[15] Modulation of the zeta potential directly reflects changes in surface chemistry and enables decoupling the effects of surface charge and binding affinity from grafting density.[33] Surface charge is a key factor governing protein affinity, orientation and catalytic accessibility upon immobilisation.[4,33]

As shown in Fig. 2D and in Table 1, semi-quantitative differences in the atomic composition of the materials can be observed, enabling the assessment of support grafting. Energy-dispersive spectroscopy (EDS) was employed to provide a semi-quantitative determination of the elemental composition of the nanoconjugates, as a widely used multielemental analytical technique for confirming elemental presence and surface composition.[34,35] Excellent colloidal stability due to strong electrostatic repulsion between particles.[32]

The MNPs@TEOS was initially validated by the detection of iron (Fe) at 12.0 At.% and silicon (Si) at 8.6 At.%, confirming the formation of a silica coating on the magnetic core. The quantification of ligands introduced onto the surface was based on the atomic percentage of silicon after functionalisation with the silanes APTS and MPTS. The results indicated that the total silane grafting density was comparable between the modified samples, with MNPs@TEOS–APTS exhibiting 14.2 At.% of Si and MNPs@TEOS–MPTS exhibiting 14.1 At.% of Si.

This analysis was crucial to establish that subsequent differences in functional performance cannot be attributed to variations in the amount of silane scaffold, but rather to the chemical nature of the terminal functional group.[36] The successful grafting of MPTS was further confirmed by the unequivocal detection of sulphur (S) at 9.1 At.%, a marker element introduced exclusively by the thiol group. The observation of similar ligand densities thus enabled the isolation of the effect of terminal functional group chemistry (amine *versus* thiol) on adsorption and catalytic processes.

Table 1 Elemental composition (At.%) of the surface-functionalized magnetic nanoparticles determined by EDX analysis. The data detail the relative abundance of silicon (Si), iron (Fe), oxygen (O), and sulfur (S) for each system, corroborating the successful incorporation of the respective organosilane linkers (TEOS, APTS, and MPTS) onto the magnetic core

Functionalization linkers	Si	Fe	O	S
TEOS	11, 6	32, 2	40, 9	0
TEOS – APTS	15, 5	42, 7	39, 1	0
TEOS – MPTS	19, 7	15, 9	30, 1	14, 4

Characterization of enzyme nanoconjugates

The immobilization efficiency was evaluated by quantifying total proteins on the surface of the functionalized nanomaterials, as shown in Fig. 3A. It can be observed that functionalization of MNPs with TEOS–APTS led to a reduction of over 5% in cellulase immobilization compared to MNPs functionalized solely with TEOS (0.96 and 1.02 mg mg^{-1}, respectively). In contrast, MNPs functionalized with TEOS–MPTS showed only a marginal increase in the amount of immobilized enzyme (1.04 mg mg^{-1}). The optimal conditions for enzymatic activity assays were determined to be pH 5 and 50 °C, as predicted in the literature.[37] As shown in Fig. 3B, the highest recorded activity (1.92 U g^{-1}) was achieved through immobilization using MNPs@TEOS–APTS, followed by MNPs@TEOS, which demonstrated the second highest activity, reaching 1.63 U g^{-1}. Surprisingly, MNPs@TEOS–MPTS, despite showing high cellulase loading, exhibited the lowest enzymatic activity values (1.61 U g^{-1}), with only a slight difference compared to the non-immobilized enzyme (0.37 U g^{-1}).

According to Sukharnikov *et al.* (2011), the structural diversity of cellulases, distributed across different glycoside hydrolase (GH) families, implies distinct modes of interaction with immobilization supports. Many of these enzymes contain cellulose-binding modules (CBMs), which are essential for substrate recognition and efficient hydrolysis.[37] Therefore, the functionalization strategy directly influences enzyme orientation, active-site accessibility, and overall catalytic performance.[22,37]

For the TEOS functionalizer linker, a high enzyme loading was observed, possibly associated with multilayer formation. Although this accumulation increases the amount of protein immobilized, it may compromise catalytic activity since the excessive enzyme density on the support surface can generate steric hindrance, restricting substrate diffusion and CBM accessibility.[22,37]

Conversely, covalent coupling *via* APTS preserved higher catalytic activity. This effect may be related to the formation of imine bonds in regions more distant from the active site and CBM, thereby maintaining substrate accessibility.[22,37] Moreover, under low pH, cellulases exhibit an overall negative surface charge, favouring electrostatic interactions with protonated amino groups of APTS. This effect may contribute to a more favourable enzyme orientation on the support.[22,37]

The MPTS strategy, in turn, promotes covalent bonding through thiol groups, conferring greater stability and reducing enzyme leaching.[22] However, this coupling may also restrict the conformational flexibility of cellulases, particularly processive enzymes that require structural mobility to slide along the cellulose chain.[22,37] Thus, although stability is enhanced, catalytic activity may be partially compromised.[22,37]

Taken together, these results highlight that the activity and stability of immobilized cellulases depend on a balance between enzyme loading, orientation, and structural flexibility.

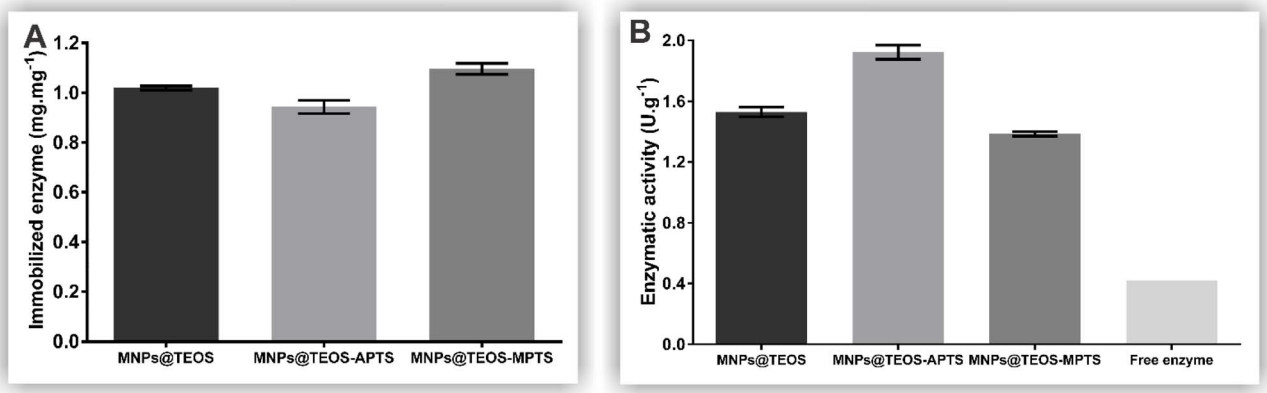

Fig. 3 (A) Relative enzyme loading capacity (mg enzyme/mg support) of cellulases immobilized on MNPs under different surface functionalization strategies; and (B) cellulolytic activity of enzyme nanoconjugates for each ligand employed.

Therefore, the choice of functionalization strategy should not rely solely on maximizing enzyme loading but also consider the structural requirements of cellulases to preserve their catalytic efficiency.[37]

Analyse of cellulase immobilization

The stability of the enzymes was evaluated by determining their catalytic activity under different pH and temperature conditions. Fig. 4 presents the catalytic activity of the cellulase

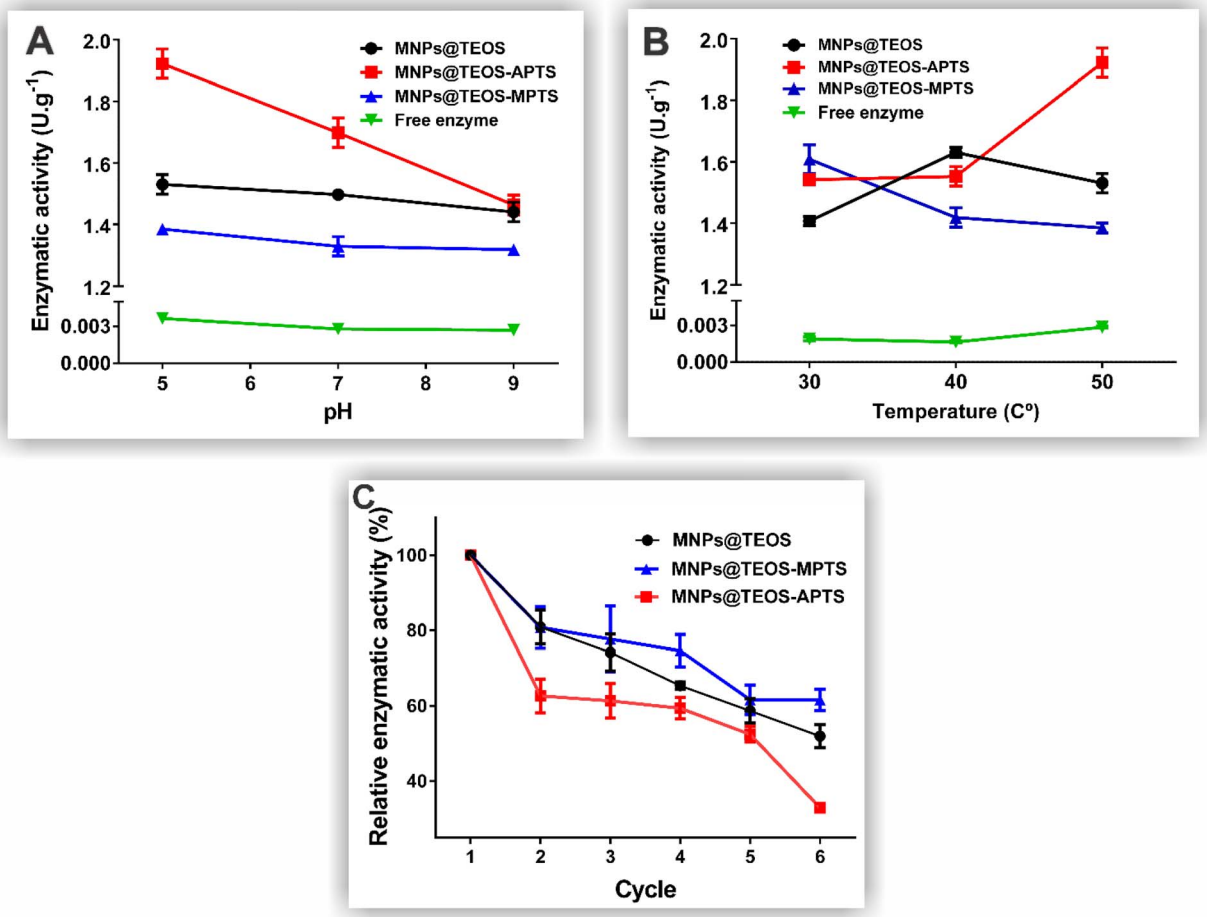

Fig. 4 Catalytic performance and operational stability of cellulases immobilized on functionalized magnetic nanoparticles (MNPs). (A) Influence of pH (5.0–9.0) on the enzymatic activity of free and immobilized cellulases. (B) Effect of temperature (30–50 °C) on catalytic activity. (C) Reusability profile (operational stability) of the immobilized biocatalysts over six consecutive reaction cycles.

enzyme as a function of pH (Fig. 4A) and temperature (Fig. 4B). MNPs@TEOS–APTS exhibited a pronounced decrease in enzymatic activity with increasing pH, showing a marked loss of activity under alkaline conditions, whereas the other bioconjugates retained comparatively higher activity across the evaluated pH range.

Regarding temperature effects, MNPs@TEOS–APTS showed a significant reduction in enzymatic activity at temperatures below 50 °C, indicating limited stability under lower-temperature conditions. In contrast, MNPs@TEOS and MNPs@TEOS–MPTS displayed distinct thermal responses, with MNPs@TEOS presenting intermediate thermal resistance and MNPs@TEOS–MPTS exhibiting impaired catalytic performance as temperature increased. The free enzyme followed a similar trend to the APTS-based system, showing reduced activity outside its optimal temperature range.

In general, the data supported the hypothesis that the glutaraldehyde imine group, which activates the APTS-functionalized MNPs, may interact with amines on the enzyme in a highly effective manner.[38] The high enzymatic activity can be attributed to the immobilization support's ability to bind to sites distant from the enzyme's active sites.[16,38] This preference is influenced by the distribution of electrical charges, where a pH close to 7 favors a predominance of negative charges, due to the greater presence of acidic amino acids compared to basic amino acids in the enzyme's structure.[16,38] Thus, the favourable charge distribution facilitates the formation of covalent bonds between the ligand and cellulase at specific enzyme sites, resulting in effective immobilization and preservation of enzymatic activity.[38] However, it is essential to note that despite this effectiveness, the enzymatic activity showed limited resistance when subjected to variations in medium conditions.

Regarding MNPs@TEOS–MPTS, the thiol groups at their ends can covalently interact with the enzyme's amine groups, providing greater stability against variations in medium conditions.[16,22] However, this strong binding may lead to inactivation of amino acids in the enzyme's active site, resulting in low catalytic activity, as also demonstrated in the molecular docking analysis.[16,22]

The activity of MNPs@TEOS was comparatively lower than MNPs@TEOS–APTS and slightly higher than MNPs@TEOS–MPTS. Additionally, MNPs@TEOS exhibited intermediate resistance to pH variation but lower stability at elevated temperatures. This difference may be attributed to the type of bond between MNPs@TEOS and the enzymes, which involves silanol groups interacting with enzyme amines.[16] These bonds likely occurred at sites distant from the enzyme's active sites, allowing the enzymes to maintain their catalytic activity.[16,22] However, these bonds are strong enough to increase the bioconjugate's resistance under various conditions, making MNPs@TEOS a promising option for practical enzyme immobilization applications.[16]

Operational stability is a decisive factor for the industrial viability of nanobiocatalysts, as it directly mitigates the costs associated with enzyme replacement.[3,36,39] The reusability profile of the immobilized cellulases over six consecutive cycles is presented in Fig. 4C. The data reveal distinct performance behaviors depending on the surface functionalization strategy.

The thiol-functionalized system (MNPs@TEOS–MPTS) exhibited the highest durability, retaining over 62% of its initial activity. This robustness is attributed to the formation of stable covalent bonds mediated by the thiol groups, which effectively minimize enzyme leaching and enhance resistance to environmental stress during repeated cycles.[15,16,37]

In contrast, the amine-functionalized system (MNPs@TEOS–APTS), despite showing the highest initial activity in previous assays (1.92 U g^{-1}), experienced a marked decline, retaining only 33% of activity after the sixth cycle.[17] This suggests that the specific orientation or interaction nature favoring initial substrate access may render the enzyme more susceptible to desorption or structural fatigue under operational conditions, highlighting a trade-off between maximal initial activity and long-term stability.[36,40]

Notably, the MNPs@TEOS system displayed an intermediate behavior, retaining approximately 50% of its initial activity.[15,16] By relying on interactions with surface silanol groups rather than additional organosilane linkers, this system demonstrates a balance between synthetic simplicity and operational resilience, maintaining significant catalytic potential without the complexity of further functionalization steps.

Enzymatic orientation and adsorption

To understand the influence of the functionalizer linker on enzyme binding efficiency and its orientation on the nanomaterial surface, an *in silico* study was conducted using molecular docking to predict and analyse the thermodynamic binding affinity and the main intermolecular interactions occurring in the cellulase-ligand binding. The energy values, binding sites, and interactions obtained for the studied complexes are presented in Table 2 and Fig. 5.

Molecular docking indicated that there is a small difference between the interaction energy values of the enzyme with the investigated functionalization linkers (Table 1). From the thermodynamic perspective, the APTS linker had the highest affinity for enzymes because the interaction energy was the lowest (−3.96 kcal mol^{-1}). In comparison, the interaction energy between MPTS linker and enzyme was −3.24 kcal mol^{-1} while that between TEOS and enzyme was −2.81 kcal mol^{-1}. The lower the binding energy value, the stronger the interaction between the enzyme and the linker.[41,42] Therefore, according to the theoretical results, we would expect the experimental adsorption tests to show that the MNPs@TEOS–APTS binds

Table 2 Binding energy between enzyme–functionalization linkers calculated by molecular docking

Functionalization linkers	Binding energy ΔG (enzyme–ligand)/kcal mol^{-1}
TEOS	−2.81
TEOS – APTS	−3.96
TEOS – MPTS	−3.24

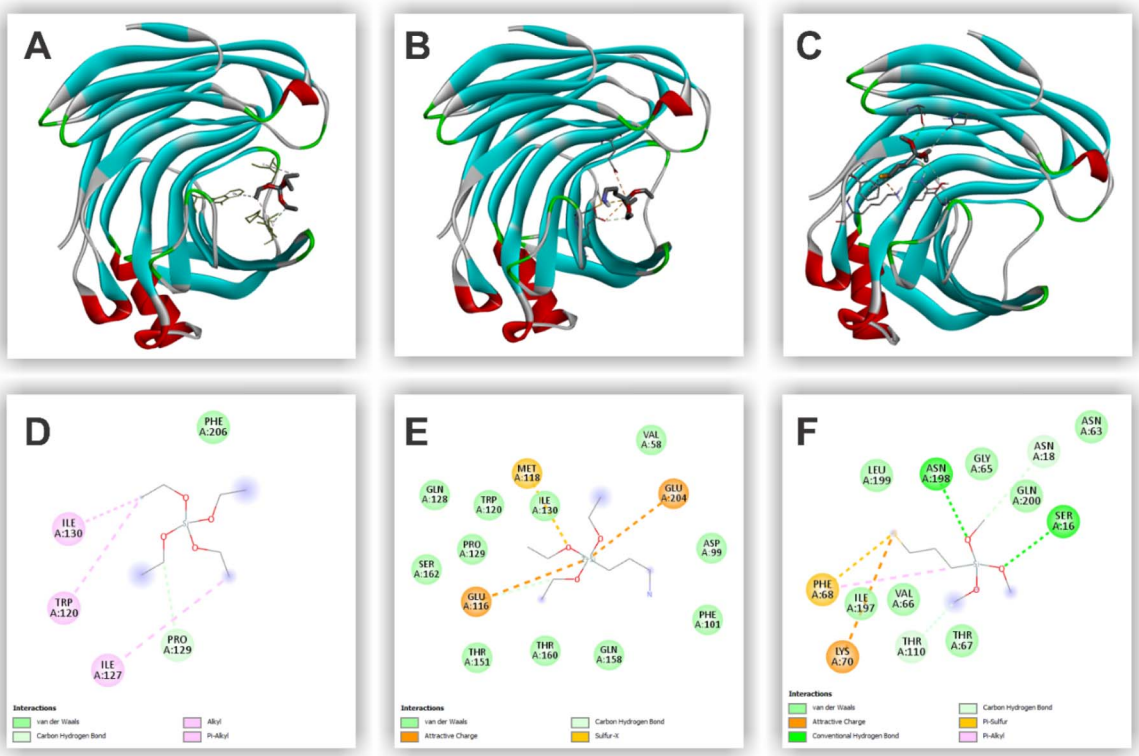

Fig. 5 Superposition of molecular docking results for (A) TEOS, (B) APTS and (C) MPTS with cellulase using AutoDock4. 2D interaction maps between (D) TEOS, (E) APTS and (F) MPTS with cellulase active site residues.

more strongly to the enzyme, followed by MNPs@TEOS–MPTS and then MNPs@TEOS.

By analysing the 3D and 2D interaction maps (Fig. 5), we can observe that the functionalization linkers interact with different regions of the cellulase enzyme. The TEOS molecule binds to the "cord region" of the enzyme, primarily interacting with residues Trp120, Ile127, Ile130, and Pro129 (Fig. 5A and D). The APTS molecule binds specifically to the enzyme's "binding cleft region" with residues Glu116, Met118, and Glu204 (Fig. 5B and E), which constitutes the cellulase's active site, where these amino acids function as the catalytic nucleophile and acid/base in the catalytic reaction.[43] The experimental results showed that MNPs@TEOS-APTS exhibited higher enzymatic, leading us to conclude that despite binding to the enzyme's active site, APTS did not cause its inactivation. The MPTS molecule binds to the enzyme's surface region, interacting with residues Ser16, Asn18, Phe68, Lys70, Thr110, and Asn198 (Fig. 5C and F). MPTS interacts with the largest number of cellulase residues through different types of chemical interactions, particularly due to the negative charge of the sulphur atom resulting from the molecule's protonation state at pH 5.0. This factor may explain the lower catalytic activity of MNPs@TEOS–MPTS.

The immobilization efficiency of cellulases on Fe_3O_4 nanoparticles was evaluated through adsorption kinetic experiments (Fig. 6A). This process is influenced by mass transfer, which provides critical parameters such as equilibrium time and reaction rate.[44] To identify the rate-limiting step of the process, the data were fitted to pseudo-first-order and pseudo-second-order kinetic models (Fig. 6B–D).

The analysis of the data reveals that MNPs@TEOS–MPTS exhibited a faster initial adsorption rate compared to the others, approaching equilibrium after just one hour of reaction and stabilizing at six hours. In this case, it is essential to emphasize that after only one hour of reaction, a $q_{exp} = 1.06$ mg mg^{-1} had already been achieved, a difference that, on a large scale, may not justify extending the reaction time by five hours. This demonstrates how kinetic analysis can strategically contribute to process optimization. MNPs@TEOS–MPTS likely achieved a high enzyme immobilization rate due to strong enzyme/support interactions generated through covalent bonds between thiol and amino groups.[16] In contrast, MNPs@TEOS–APTS initially exhibited a slower immobilization rate, possibly due to a selective interaction mechanism between glutaraldehyde-activated APTS-functionalized particles and cellulases.[39,45]

Regarding the adsorption kinetic models (Table 3), the pseudo-first-second-order model best represented the adsorption of MNPs@TEOS ($R^2 = 0.984$). Although the R^2 value was very close to that of the pseudo-first-order model ($R^2 = 0.980$), the pseudo-second-order model yielded a $q_e = 1.01$ mg mg^{-1}, much closer to the experimental $q_{exp} = 1.04$ mg mg^{-1}, indicating better adaptability of this model. Thus, it can be inferred that the adsorption step at active sites may be the predominant phase in this case.[46]

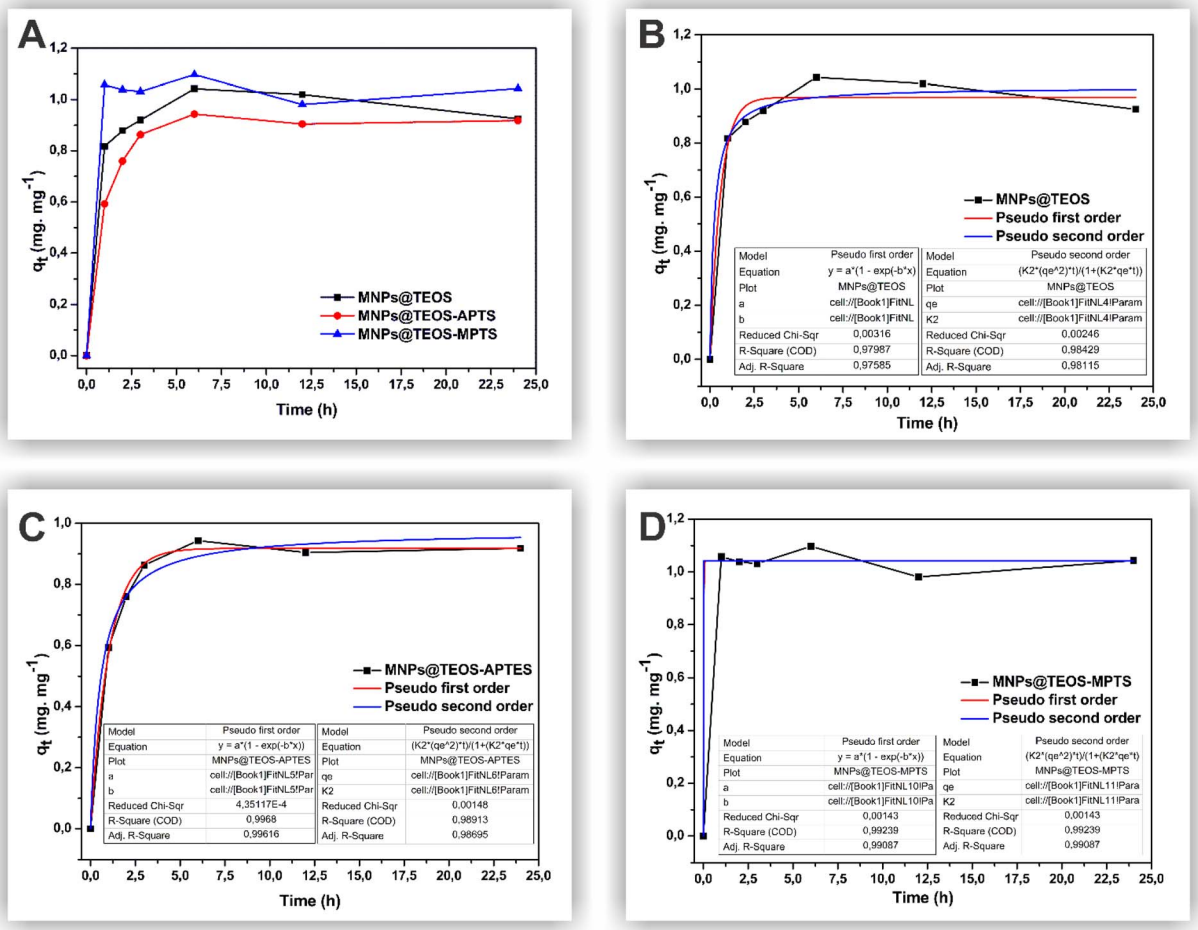

Fig. 6 (A) Adsorption kinetic of cellulases by naked and functionalized Fe_3O_4; (B) adsorption kinetic of cellulases by MNPs@TEOS: experimental data, and pseudo-first and pseudo-second order models; (C) adsorption kinetic of cellulases by MNPs@TEOS–APTS: experimental data, and pseudo-first and pseudo-second order models; (D) adsorption kinetic of cellulases by MNPs@TEOS–MPTS: experimental data, and pseudo-first and pseudo-second order models.

Table 3 Kinetic parameters obtained from the adsorption of cellulases to MNPs@TEOS, MNPs@TEOS–APTS, and MNPs@TEOS–MPTS

Models	Parameters	MNPs@TEOS	MNPs@TEOS–APTS	MNPs@TEOS–MPTS
Pseudo-first order	q_{exp} (mg mg^{-1})	1.04	0.94	1.10
	q_e (mg mg^{-1})	0.97	0.92	1.04
	K_1 (min^{-1})	1.69	0.97	62.79
	R^2	0.980	0.997	0.992
Pseudo-second order	q_e (mg mg^{-1})	1.01	0.98	1.04
	K_2 (mg min^{-1} mg^{-1})	4.19	1.82	9.42 × 1029
	R^2	0.984	0.989	0.992

In contrast, for MNPs@TEOS–APTS, the pseudo-first-order model provided the best fit (R^2 = 0.997), indicating that external diffusion, typically governing the initial stage, dominates the adsorption process.[47] For MNPs@TEOS–MPTS, both models exhibited good agreement, with R^2 = 0.992 and q_e = 1.04 mg mg^{-1}. It is essential to note that while kinetic models permit certain assumptions about the adsorption mechanism, they do not independently describe each step of the adsorption process (Saleh, 2022a).

Conclusions

Cellulases were successfully immobilised on TEOS coated Fe_3O_4 nanoparticles functionalised with APTS and MPTS, and the effect of ligand chemistry on adsorption, activity and reusability was systematically evaluated. MNPs@TEOS–MPTS showed the highest immobilisation capacity (q_e = 1.06 mg mg^{-1}) and fastest adsorption kinetics, reaching equilibrium within 1 h, while MNPs@TEOS and MNPs@TEOS–APTS presented slightly lower

capacities (q_e = 1.04 and 0.94 mg mg^{-1}, respectively). MNPs@TEOS–APTS exhibited the highest catalytic activity (1.92 U g^{-1}) under optimal conditions (pH 5, 50 °C) but suffered a pronounced activity loss under alkaline conditions. In contrast, MNPs@TEOS–MPTS displayed lower initial activity (1.61 U g^{-1}) but superior thermal resistance and operational stability. Reusability assays confirmed MNPs@TEOS–MPTS as the most robust system, retaining 62% of its activity after six cycles, whereas MNPs@TEOS–APTS retained only 33%. The non-functionalised MNPs@TEOS showed intermediate behaviour (52% retention). Molecular docking analysis corroborated the experimental trends, indicating higher binding affinity for APTS and more stabilising surface interactions for MPTS, explaining the trade-off between catalytic efficiency and stability. Overall, these findings demonstrate that ligand selection critically determines the balance between activity and durability, with APTS favouring high initial reaction rates, MPTS enabling enhanced operational stability and reusability, and TEOS providing an intermediate performance.

Author contributions

JPO conceived the project. LLB, TAS and CCM performed the experiments, characterizations, and analysis. LLB, ACLB and JPO wrote the paper, JNSF and ARS performed the docking molecular, STAC, LMP and RG revised the writing of the manuscript. JPO guided the research.

Conflicts of interest

The authors declare that they have no competing interests.

Data availability

All data supporting this study have been included in the article.

Acknowledgements

This work was supported by the Fundação de Amparo à Pesquisa e Inovação do Espírito Santo (FAPES, Brazil). The authors acknowledge the use of equipment and facilities at the Laboratório de Ultraestrutura Carlos Alberto Redins (LUCCAR, UFES, Brazil), the Multi-user Laboratory for Biomolecular Analysis (CCS/UFES, Brazil), the Laboratório de Materiais Carbonosos e Cerâmicos (LMC, UFES, Brazil), and LabPetro (UFES, Brazil), and thank all laboratories for providing technical support for the experiments.

References

1 A. K. Patel, R. R. Singhania, S. J. Sim and A. Pandey, *Bioresour. Technol.*, 2019, **279**, 385–392.
2 A. Dadwal, S. Sharma and T. Satyanarayana, *Int. J. Biol. Macromol.*, 2021, **188**, 226–244.
3 K. N. Rajnish, M. S. Samuel, S. Datta, N. Chandrasekar, R. Balaji, S. Jose and E. Selvarajan, *Int. J. Biol. Macromol.*, 2021, **182**, 1793–1802.
4 S. H. Hosseini, S. A. Hosseini, N. Zohreh, M. Yaghoubi and A. Pourjavadi, *J. Agric. Food Chem.*, 2018, **66**, 789–798.
5 L. Zang, J. Qiu, X. Wu, W. Zhang, E. Sakai and Y. Wei, *Ind. Eng. Chem. Res.*, 2014, **53**, 3448–3454.
6 K. Khoshnevisan, F. Vakhshiteh, M. Barkhi, H. Baharifar, E. Poor-Akbar, N. Zari, H. Stamatis and A. K. Bordbar, *Mol. Catal.*, 2017, **442**, 66–73.
7 I. N. Ahmed, R. Chang and W. B. Tsai, *Colloids Surf., B*, 2017, **152**, 339–343.
8 S. Kumar, V. Morya, J. Gadhavi, A. Vishnoi, J. Singh and B. Datta, *Heliyon*, 2019, **5**, e01702.
9 W. Huang, S. Pan, Y. Li, L. Yu and R. Liu, *Int. J. Biol. Macromol.*, 2020, **162**, 845–852.
10 J. Yi, M. Qiu, Z. Zhu, X. Dong, E. Andrew Decker and D. J. McClements, *Food Chem.*, 2021, **364**, 130447.
11 A. Javid, H. Amiri, A. T. Kafrani and H. Rismani-Yazdi, *Int. J. Biol. Macromol.*, 2022, **207**, 324–332.
12 M. Guo, J. Zhao, S. Han, J. Xu, X. B. Yin and M. Zhang, *Colloids Surf., A*, 2025, **724**(5), 137448.
13 X. Xu, J. Xu, N. Lu and M. Zhang, *Langmuir*, 2025, **41**, 27537–27546.
14 Y. Chen, H. Li, J. Xu, X. B. Yin and M. Zhang, *Langmuir*, 2025, **41**, 13645–13654.
15 T. de Andrade Silva, W. J. Keijok, M. C. C. Guimarães, S. T. A. Cassini and J. P. de Oliveira, *Sci. Rep.*, 2022, **12**, 6815.
16 B. Thangaraj, Z. Jia, L. Dai, D. Liu and W. Du, *Arab. J. Chem.*, 2019, **12**, 4694–4706.
17 G. L. Miller, *Anal. Chem.*, 1959, **31**, 426–428.
18 T. Sokač, A. Šalić, A.-M. Dukarić, M. Tišma, M. Planinić, B. Zelić and M. Božinović, *Croat. J. Food Sci. Technol.*, 2023, **15**, 151–162.
19 H. Zhang, Z. Fan, J. Li and L. Han, *Bioresour. Technol.*, 2019, **282**, 384–389.
20 D. Q. Hung, L. X. Dinh, N. Van Tung, L. T. M. Huong, N. T. Lien, P. T. Minh and T.-H. Le, *Results Chem.*, 2023, **6**, 101095.
21 M. P. Desai and K. D. Pawar, *Mater. Sci. Eng., C*, 2020, **106**, 110169.
22 T. de Andrade Silva, W. J. Keijok, M. C. C. Guimarães, S. T. A. Cassini and J. P. de Oliveira, *Sci. Rep.*, 2022, **12**, 6815.
23 I. Šimkien, M. Treideris, G. Niaura, R. Szymczak, P. Aleshkevych, A. Rza, I. Kašalynas, V. Bukauskas and G. J. Babonas, *Mater. Chem. Phys.*, 2011, **130**, 1026–1032.
24 M. Muzzio, J. Li, Z. Yin, I. M. Delahunty, J. Xie and S. Sun, *Nanoscale*, 2019, **11**, 18946–18967.
25 M. Sadeghi, Z. Moghimifar and H. Javadian, *Chem. Phys. Lett.*, 2023, **16**, 140161.
26 M. Kotera, A. G. McDonald, S. Boyce and K. F. Tipton, *PLoS One*, 2008, **3**, e1537.
27 D. Bersani, P. P. Lottici and A. Montenero, *J. Raman Spectrosc.*, 1999, **30**, 355–360.
28 S. Saremi-Yarahmadi, K. G. U. Wijayantha, A. A. Tahir and B. Vaidhyanathan, *J. Phys. Chem. C*, 2009, **113**, 4768–4778.
29 S. D. A. Zaidi, C. Wang, B. György, C. Sun, H. Yuan, L. Tian and J. Chen, *J. Colloid Interface Sci.*, 2020, **569**, 164–176.
30 D. Zhang, H. E. Hegab, Y. Lvov, L. Dale Snow and J. Palmer, *Springerplus*, 2016, 48.

31 B. Stuart, *Infrared Spectroscopy Fundamentals and Applications*, 2004, vol. 1.
32 T. Mudalige, H. Qu, D. Van Haute, S. M. Ansar, A. Paredes and T. Ingle, in *Nanomaterials for Food Applications*, Elsevier, 2018, pp. 313–353.
33 B. P. Dwivedee, S. Soni, R. Bhimpuria, J. K. Laha and U. C. Banerjee, *Int. J. Biol. Macromol.*, 2019, **133**, 1299–1310.
34 R. Dewolfs, R. De Neve and F. Adams, *Anal. Chim. Acta*, 1975, **75**, 47–60.
35 J. Ashwini John, M. S. Samuel and E. Selvarajan, *Fuel*, 2023, **1**(Part 1), 126364.
36 Q. Chen, D. Liu, C. Wu, K. Yao, Z. Li, N. Shi, F. Wen and I. D. Gates, *Bioresour. Technol.*, 2018, **263**, 317–324.
37 L. O. Sukharnikov, B. J. Cantwell, M. Podar and I. B. Zhulin, *Trends Biotechnol.*, 2011, **29**, 473–4792011.
38 L. T. Izrael Živković, L. S. Živković, B. M. Babić, M. J. Kokunešoski, B. M. Jokić and I. M. Karadžić, *Biochem. Eng. J.*, 2015, **93**, 73–83.
39 S. S. Rashid, A. H. Mustafa, M. H. A. Rahim and B. Gunes, *Int. J. Biol. Macromol.*, 2022, **209**, 1048–1053.
40 M. R. Ladole, J. S. Mevada and A. B. Pandit, *Bioresour. Technol.*, 2017, **239**, 117–126.
41 S. Q. B. Gonçalves, E. A. Da Silva Filho, O. V. De Oliveira and A. d. S. Gonçalves, *Rev. Ifes Ciênc.*, 2020, **6**, 73–83.
42 A. S. d. A. Segantine and A. d. S. Gonçalves, *Rev. Ifes Ciênc.*, 2020, **6**, 262–278.
43 S. Khademi, D. Zhang, S. M. Swanson, A. Wartenberg, K. Witte and E. F. Meyer, *Acta Crystallogr., Sect. D:Biol. Crystallogr.*, 2002, **58**, 660–667.
44 T. A. Saleh, *Interface Science and Technology*, 2022, vol. 34, pp. 99–126.
45 J. de Souza Lima, F. N. Costa, M. A. Bastistella, P. H. H. de Araújo and D. de Oliveira, *Bioprocess Biosyst. Eng.*, 2019, **42**, 1165–1173.
46 T. A. Saleh, in*Interface Science and Technology*, 2022, vol. 34, pp. 65–97.
47 J. Wang and X. Guo, *J. Hazard. Mater.*, 2020, **390**, 122156.